Master project, 2014, Microengineering

Nanoparticle assembly : scalable process development from nanoscale molding to hardware/software implementation

By Kevin Müller
Supervised by Valentin Flauraud
Project director : Prof. Jürgen Brugger
Submitted on 20.06.2014

Microsystems laboratory 1 (LMIS1)
ÉCOLE POLYTECHNIQUE
FÉDÉRALE DE LAUSANNE

Initial description of the project

Gold colloids will be assembled in a nanoscale template in order to enhance single molecule fluorescence. Capillarity assisted nanoparticle assembly will be optimised both in terms of substrate properties and process parameters allowing high yield assembly with minimal gap variations. The templates will be fabricated in a transparent material compatible with optical measurements and characterized with SEM and AFM. The optical measurements will be performed using a high speed state of the art sCMOS camera allowing larger scale parallel mapping of the fluorescence signal over a broad number of antennas.

Nanoparticle assembly : scalable process development from nanoscale molding to hardware/software implementation

Kevin Müller, Microengineering

Assistant: *Valentin Flauraud*
Professor: *Jürgen Brugger*

In this work, templates for capillary assisted particles assembly (CAPA) are fabricated by molding with Ormocer, a transparent and non-conductive UV-curable polymer. Overall, the shape of the structures was successfully replicated and the silicon master is reusable more than six times without damage. However, the main issue of this process is the widening of the structures, leading to multiple nanospheres per hole instead of one.

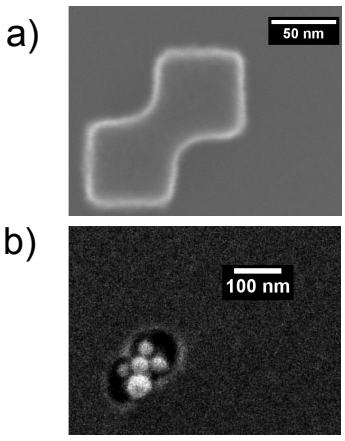

a) Structure on Silicon
b)Structure molded from a) on Ormocer filled with multiple nanospheres

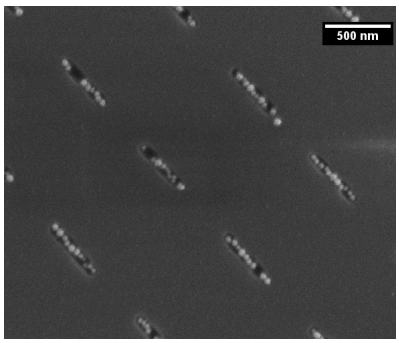

Rectangles filled with nanospheres

Additionally, the setup for CAPA has been improved with a Labview program and an Arduino shield. The Labview program allows the control of three different motors and a Peltier element and sensors to monitor the temperature of the patterned chip, the temperature and the humidity of the room. All the data collected by the program is written in a text file that can be read by other program such as MatLab. The Arduino shield is based on a previous design. The additional features consists in a H-bridge to change the polarity of the Peltier and a connector for a power supply that can deliver a current of 10 A instead of 5 A.

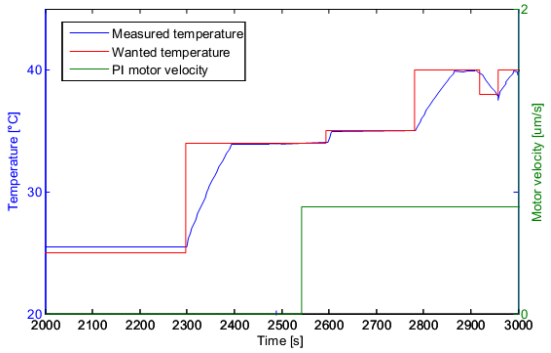

Plots of the measured temperature, the wanted temperature and the PI motor velocity monitored by the Labview program.

Finally, the Rose Bengal fluorescent dye has been theoretically investigated for future fluorescence enhancement experiment using nanosphere dimers.

Table of contents

1. Introduction

When one wants to fabricate metal nanostructures for plasmonic effects, e-beam lithography [13] or similar process such as focused ion beam milling [14,15], are typically used to fabricate structure with sub 100 nm feature size but those process are expensive and have low throughput. On the other hand, capillary assisted particle assembly (CAPA) is a templated self-assembly process that allows accurate positioning of nanoparticles on a nanostructured template that can be produced by molding. In addition, since nanospheres and nanorods are now commercially available, CAPA is even more attractive. By using CAPA with gold nanoparticles, cost eficient process with a high throughput can be developed to fabricate plasmonic nanostructures such as nanosphere dimers. If the gap between two nanospheres is below 20 nm, an intensity enhancement higher than 50-fold can be observed in the gap leading to fluorescent enhancement up to 1340-fold [19] when a fluorescent dye with low quantum yield is placed in the gap.

In this work, CAPA is used to place gold nanosphere with a diameter of 50 nm in an Ormocer template produced by molding. The objective is to control the size of gap between two nanospheres and ultimately illustrate the size of the gap by measuring the fluorescence enhancement of the Rose Bengal fluorescent dye. Moreover, the experimental setup for the CAPA is improved thanks to a Labview program and a new Arduino shield. The Labiew program enables the control of three motors and a Peltier element, reads two different sensors and monitors the temperature, the humidity and the velocity during the CAPA. The new Arduino shield can be connected to a power supply that can deliver twice the current compare to the previous design and an H-bridge has been added in order to commute the polarity of the Peltier and enable negative temperature regulation.

2. Theory

2.1. Capillary assisted particle assembly (CAPA)

The capillary assisted particle assembly (CAPA) consists in the assembly of particles on a structured and hydrophobic template using the capillary force applied by the meniscus. A CAPA process consists in the dragging of a colloidal solution confined between a slide and a chip with a patterned surface (Figure 1). The particles are deposited on the chip while the glass slide is moving. The contact angle, the capillary forces and the evaporation rate and the formation of the accumulation region are key factors for CAPA.

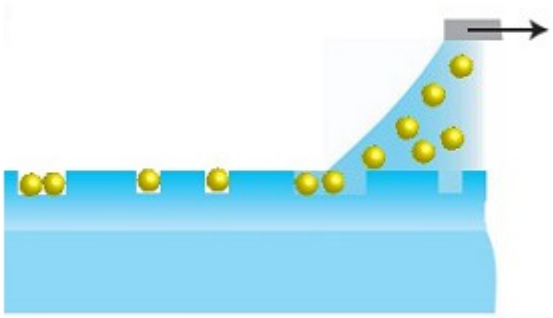

Figure 1 : Illustration of CAPA. The gold particles contained in the liquid are deposited in the holes of the template. [1]

2.1.1 Contact angle and capillary forces

The contact angle is the angle between a liquid-gas interface and the solid-liquid interface and it determines the wettability of the surface. If the contact angle is lower than 90°, the surface is considered hydrophilic and hydrophobic otherwise. This contact angle depends mainly of the surface tension of the different interfaces. For more accurate analysis, the roughness, the chemical uniformity on the surface and other forces applied to the meniscus have to be considered.

Usually, for CAPA, the slide and the chip are hydrophobic and the colloidal solution consists of water, particles and a controlled amount of surfactant. For the contact angle between the chip and the liquid-gas interface, the Young's equation predicts the relationship between the contact angle at equilibrium θ, the surface tension of the liquid-gas interface γ_{lg}, the surface tension of the solid-gas interface γ_{sg} and the surface tension of the solid-liquid interface γ_{sl} as follows :

$$\gamma_{sg} = \gamma_{sl} + \gamma_{lg}\cos(\theta) \quad (1)$$

The surfactants decrease the surface tension of the liquid-gas and the solid-liquid interfaces, decreasing the contact angle.

When this equality isn't respected, a force is applied at the three phase contact line parallel to the surface tension of the liquid-solid and solid-gas interfaces. Hence, when a force is applied to the meniscus, the contact angle reaches an other equilibrium where the sum of the forces becomes zero. Moreover, the roughness and the speed of the meniscus on the surface has an effect on the contact angle[2] leading to a contact angle hysteresis defined by its extreme values : the receding angle and the advancing angle.

When the meniscus goes over a flat surface, the capillary force applied by the meniscus must be large enough to drag the particle. Therefore, if the contact angle is too small, particles are deposited on the surface. When the meniscus passes over a hole, the meniscus is bent and pushes the particle into the hole (Figure 2). In this case, the probability to find a particle in the hole decreases when the contact angle increases but, on the other hand, if the contact angle is too low, the particles start to be deposited outside the patterned area.

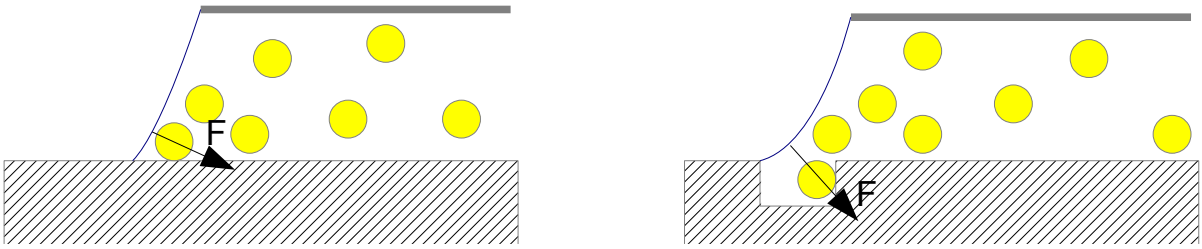

Figure 2 : Force applied on the gold spheres by the meniscus.

At the edge of the slide, the three phase contact line is pinned because the surface tension of the solid-gas and solid-liquid interfaces are higher than the surface tension of the gas-liquid interface. Hence, a force has to applied to unpin the three phase contact line.

2.1.2. Evaporation rate and accumulation

When water is in contact with air, there is evaporation or condensation. The evaporation rate or the condensation rate depends on the temperature of the liquid and the temperature and humidity

of the surrounding air. When there is no evaporation or condensation, it means that the temperature of the liquid corresponds to the dew point. Some formulas have been found to approximate the dew point from the humidity and the temperature of the air [3]. A simple and still accurate formula is the Magnus formula :

$$\gamma_m(T, RH) = \ln\left(\frac{RH}{100}\right) + \frac{bT}{c+T}$$
$$T_{dp}(T, RH) = \frac{c\,\gamma_m(T, RH)}{b - \gamma_m(T, RH)} \quad (1)$$

RH is the relative humidity in percent, T is the temperature of the air and *b* and *c* are constants. Those values of the constants give accurate result when the temperature is between 0°C and 50°C (error smaller than 0.05%)[3] :

$$b = 17.368, c = 238.88\,°C \quad (2)$$

Since the liquid is trapped between two surfaces, the evaporation occurs only at the side of the drop. However, the three phase contact line at the edge of the slide is pinned and the contact angle between the chip and the gas-liquid interface can change only to a small extent. Therefore, due to the evaporation of the water, a flow in the colloidal solution compensates the liquid loss due to evaporation. Moreover, a flow is created when the slide is moving due to the no-slip condition of the liquid-solid interface (Figure 3). This flow becomes negligible compare to the flow due to the evaporation when the evaporation rate is high and the slide velocity is slow.

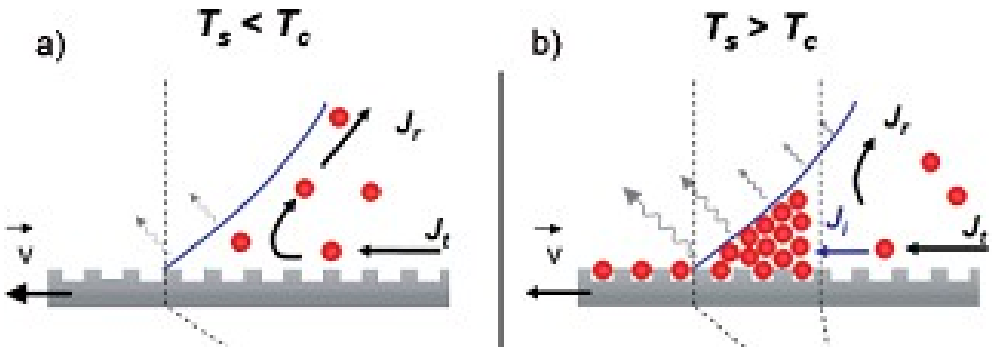

Figure 3 : Illustration of the influence of the temperature on the flows present in the liquid. J_t is flow coming from the bulk liquid that drag the particles to the meniscus and J_r is the recirculation flow that drags the partciles to the bulk liquid. a) Due to low temperature, the evaporation rate is too low so J_t is mainly due to the no-slip condition between the chip and the liquid. In this case, the recirculation flow J_r is similar to J_t which prevents the formation of an accumulation region. b) The temperature is large enough to have a high evaporation rate. In this case, the recirculation flow J_r is weak compared to J_t leading to the formation of the accumulation region.[4]

The figure 4 is a flow simulation of the system computed by W. Heiko et al[1]. Due to the flows in the liquid, the particles are dragged to the meniscus resulting in accumulation which is compensated by the diffusion due to the gradient concentration created in the liquid. Hence, there is an equilibrium between the Stokes drag, which depends mainly of the evaporation rate, the diffusion and the loss of particles due to deposition on the surface.

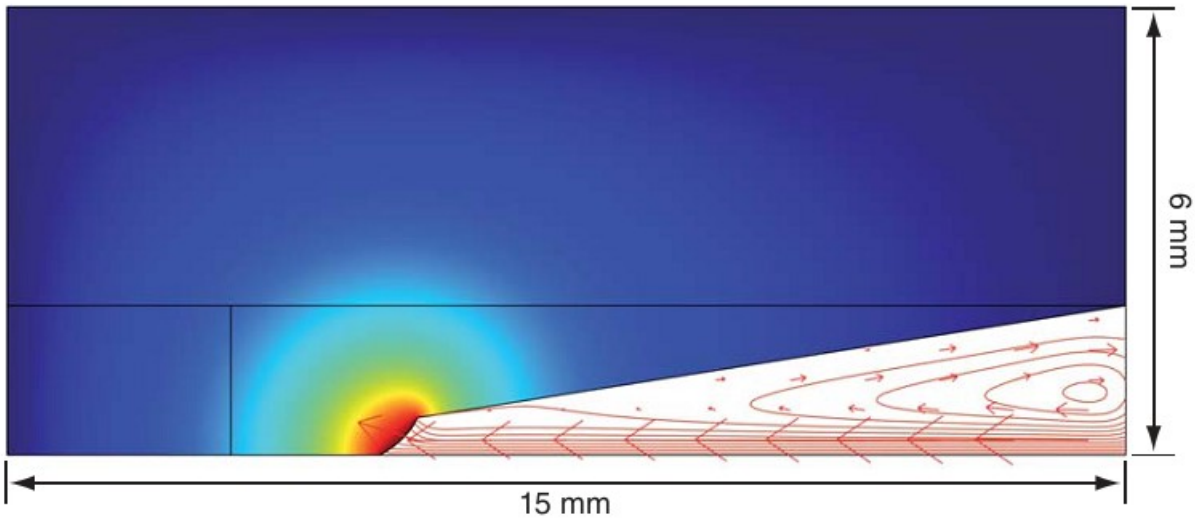

Figure 4 : Flow simulation of the system. The liquid is in white and the air is in color. The upper boundary of the liquid is separated by an impermeable barrier. The arrows show the direction of the flows.[1]

The accumulation region is crucial for a good CAPA. The high concentration of particles and, therefore, the resulting loss of mobility increase dramatically the probability that a particle is trapped in the structure on the surface. Moreover, the self-pinning of the accumulation region increases the force on the meniscus, decreasing the contact angle. However, if an inappropriate surfactant is chosen, the particle can stick to the surface, agglomerate or a repulsive force occurs between the particle and the surface, which are a disadvantage for the CAPA.[1]

2.1.3 State of the art

H. Wolf and his group have extensively studied this field. They perform the CAPA on PDMS template with gold and PS nanospheres with a diameter ranging from 60 nm to 500 nm as well as gold nanorods. They found that an assembly yield of 95% and higher can be reached when the contact angle is between 50° and 60°. Triton X-45 or CTAB are used as surfactant and the velocity of the slide is around 1 um/s[1, 3, 5]. They found that the influence of the velocity on the process is small if the velocity is sufficiently slow.

Other similar self-assembly processes have been done. In one of them, the template is placed vertically in the colloidal solution containing gold nanosphere with diameter lower than 50 nm or particles with complex shape, and the particles are deposited when the liquid evaporates. The contact angle for good assembly yield is between 10° and 30°[6].

An other process is to place the colloidal solution containing the nanospheres between the structured template and a glass chip while the particle are deposited when the meniscus passes over the structure because of the evaporation of the liquid [7]. A similar technique has been used for the assembly of particles in order to measure plasmonic effects and the measured receding contact angle was between 24° and 37° during the self-assembly process [8].

2.2 Localized plasmonic resonance

A localized plasmonic resonance is a non-propagating excitation of free electrons [9]. When an electromagnetic wave reaches a metal structure, the electrons are affected by the electric field and those that are in the conduction band, are accelerated and move in the opposite direction of the electric field. The net displacement of the electrons creates multipole moments in the structure and, due to the electrostatic forces, the electron gas tends to come back to its initial position[10]. This displacement of the electrons is an oscillation characterized by a frequency which corresponds to the plasmonic resonance and depends of the metal, the geometry of the structure, the surrounding medium and the type of multipolar oscillations. The strongest and most widely observed resonance of a nanosphere is due to a single dipolar oscillation and it is the lowest resonant frequency. When the frequency of the incident light corresponds to a resonant frequency, the corresponding multipolar oscillation can be greatly enhanced and the structure scatters efficiently the incident light.

For two nanospheres 10 nm to each other, the presence of charge on both side of the gap lead to a very high intensity enhancement in a confined area. Moreover, the intensity enhancement depends exponentially on the gap size. Such hot spot can lead to nonlinear effects[11] or can be used to perform optical trapping, surface-enhanced Raman spectroscopy[12] and fluorescent enhancement.

2.2.1 State of the art

In many cases, the plasmonic structures are fabricated using e-beam lithography[13] or focused ion beam[14, 15]. Those process are adequate for research because a high variety of shape can be prototyped but those process are expensive and have low throughput.

Rivera and al. used a self-assembly process based on colloid to place particles in the structure with the purpose of measuring their plasmonic resonance [8]. The structures that they produced were a line of 2 to 5 particles and a tripod structure formed by 4 particles.

Other interesting self-assembly processes exist, such as the fabrication of a dense array of Ag particles on a porous surface due to surface tension[16] and the self-assembly of a nanosphere dimer bound to functionalized DNA strands [17].

2.3 Fluorescent enhancement

The fluorescence is the emission of light after absorption and the mechanism leading to this phenomenon is described by the figure 5.

The phenomenon of plasmonic-enhanced fluorescence is well described by O. Martin et al [18] and some results will be exposed here. When the fluorescent dye is in a hot spot of a plasmonic structure, the excitation is greatly increased due to the intensity enhancement. Moreover, the emission rate increases because the local density of optical states is enhanced. The enhancement factor can be written as :

$$G = \frac{F_{exc} F_{rad} \left(I^o \tilde{\sigma} + \gamma_{em}^o / \phi_m^o \right)}{I^o \tilde{\sigma} F_{exc} + \gamma_{em}^o \left(1/\phi_m^o - 1 + F_{rad} + F_q \right)} \quad (3)$$

With :

$$\tilde{\sigma} = \frac{\sigma}{E_{abs}}, F_{exc} = \frac{I}{I^o}, F_{rad} = \frac{\gamma_{rad}}{\gamma^o_{em}}, F_q = \frac{\gamma_q}{\gamma^o_{em}} \quad (4)$$

Where I^o and γ^o_{em} are, respectively, the incident light intensity and the emission rate without the plasmonic structure, ϕ^o_m is the intrinsic quantum yield, σ is the absorption cross-section, E_{abs} is the energy of the absorbed photon, I, γ_{rad} and γ_q are, respectively, the intensity, the radiative emission rate and plasmonic quenched component of the emmission rate due to the presence of the plasmonic structure. Two special case can be observed. If the intrinsic quantum yield is equal to1, the equation (3) becomes :

$$G = \frac{F_{exc} F_{rad} (I^o \tilde{\sigma} + \gamma^o_{em})}{I^o \tilde{\sigma} F_{exc} + \gamma^o_{em} (F_{rad} + F_q)} \quad (5)$$

When F_{exc}, F_{rad} and F_q are multiplied by a factor, the enhancement factor is multiplied by the same factor. However, if the intrinsic quantum yield is close to 0, the equation (3) becomes :

$$G = F_{exc} F_{rad} \quad (6)$$

When F_{exc} and F_{rad} are multiplied by a factor, the enhancement factor is multiplied by the square of this factor. Hence, the fluorescent enhancement is higher when the quantum yield of the fluorescent dye is low.

F_{exc} and F_{rad} is equal to the intensity enhancement due to the plasmonic structure at the excitation wavelength and the emission wavelength, respectively. Hence, the fluorescence enhancement that can be observed in the gap of the plasmonic structure is very sensitive of the gap size.

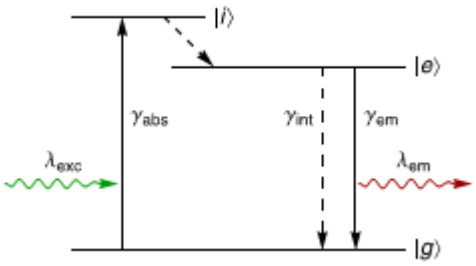

Figure 5 : Diagram representing the fluorescence mechanism. When an electron is in the ground state $|g\rangle$ and it absorbs a photon with a excitation wavelength of λ_{exc} and a absorption rate γ_{abs}, the electron is excited to the intermediate stat $|i\rangle$ following by a non-radiative decay to the excited stat $|e\rangle$. Then, the electron can relax to the ground state non- radiatively with a decay rate γ_{int} or by emitting a photon with an emission wavelength of λ_{em} and a decay rate γ_{em}.[18]

2.3.1 State of the art

Large fluorescence enhancements has been observed. For exemple, W. E. Moerner et al. observed a fluorescence enhancement of TPQDI dyes up to 1340-fold using bowtie antenna with a gap of 14 nm [19].

J. Wenger and his group decreases the background signal by placing the plasmonic nanostructure in a nanoscale hole. The fluorescent enhancement of Alexa fluor 647 with a quencher was up to 1100-fold and the gap was 15 nm [14].

With the nanosphere dimer with a gap of 23 nm bound on DNA strands, The obtained fluorescent enhancement reached 117-fold with ATTO 647 N dye [17].

3. Simulation of a nanosphere dimer

3.1 Introduction to the MNPBEM toolbox

To simulate the plasmonic resonance of the nanosphere dimer in water, the matlab toolbox MNPBEM is used [20]. This simulation tool uses a boundary element approach (BEM) developed by Garcia de Abajo and Howie [21,22]. Hence, in order to compute the charge at the surface of the plasmonic nanoparticles, the surface of the nanoparticles is discretized, the illumination with its polarization is described and the dielectric functions of the particle and the embedding medium are given. Once the charge at the surface is computed, the scattering cross-section, the absorption cross-section and the electric field at any point can be known.

3.2 Simulation results

To simulate the nanosphere dimer, each nanosphere is discretized using 2592 rectangles (Figure 6), the dielectric functions is taken from P. Johnson, and R. Christy [23] and the embedding medium is water so its dielectric constant is 1.77. The BEM solver that computes the full Maxwell equations is used. Hence, the retardation effect is taken into account. From the simulation, the scattering cross-section is computed for wavelengths from 450 nm to 650 nm and for gap size from 5 nm to 20 nm (Figure 7 a)). Then, the resonant wavelength, which is the wavelength where the scattering cross-section is maximal, is estimated. The relationship between the resonance wavelength and the gap size is plotted in the Figure 7 b).

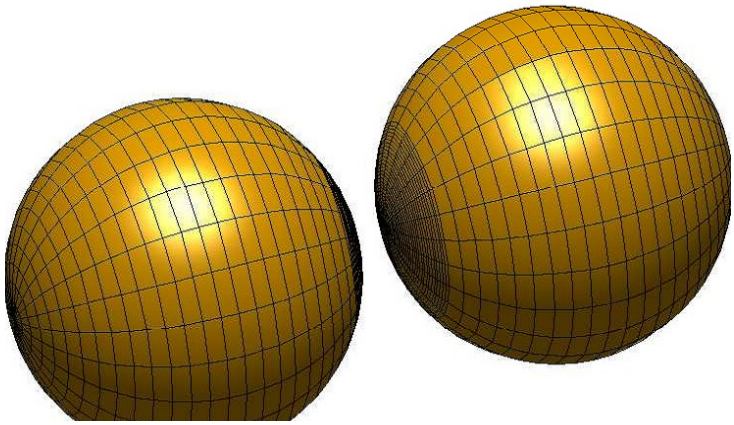

Figure 6 : Discretization of a nanosphere dimer with 2592 rectangles. The surfaces close to the gap are described with more rectangles than the rest of the sphere.

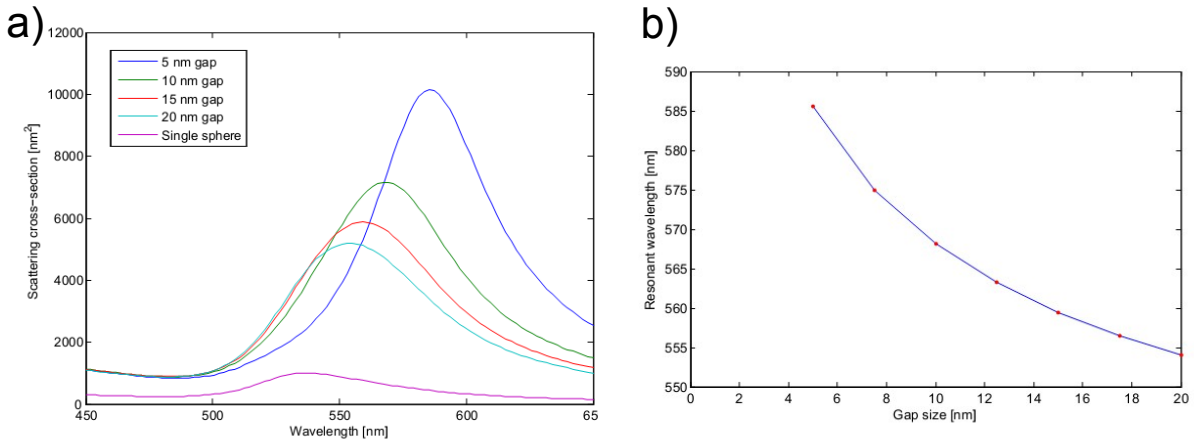

Figure 7 : a) relationship between the wavelength and the scattering cross-section for different gap size or for a single sphere. b) Relationship between the gap size and the resonant wavelength.

3.3 Choice of the fluorescent dye

For the best performance, the resonant wavelength must lie between the absorption wavelength and the emission wavelength of the fluorescent dye and the quantum yield must be low. In this work, since different gap size can be present, a good performance can be reached if the emission and the absorption wavelength of the fluorescent dye lie between 540 nm and 600 nm. For convenience, the fluorescent dye should be soluble in water.
From T. Tsai et al.[24], the emission wavelength of the Rose Bengal fluorescent dye is 548.5 nm, the absorption wavelength is 565.8 nm and the quantum yield is 0.6%. Moreover, the Rose Bengal is soluble in water and it is a common fluorescent dye. Hence, the Rose Bengal is a good candidate for fluorescence enhancement using nanosphere dimers.

4. Experimental setup

Description of the experimental setup done by Valentin Flauraud (Figure 8) :
1 : Area where the CAPA is taking place. The glass slide can be moved up and down and the chip is held using vaccum.
2 : The motor PLS-85 from PI miCos (called PI motor) can have a very low speed without vibration and is designed for high precision application. This motor allows to move the stage where the chip is and it is used for moving the slide during the CAPA.
3 : Motorized xy-stage from Standa (called Standa motors) allows to move the entire stage under the microscope.
4 : A Peltier element is used to control the CAPA by heating the chip.
5 : The temperature sensor is placed on a dummy chip such that the measured temperature is similar to the temperature of chip used in the CAPA.
6 : A microscope from Zeiss mounted with a camera from Hamamatsu is used to find the structures on the chip and observe the accumulation region during the CAPA.
7 : A camera from iDS is used to observe the contact angle during the CAPA.
8 : The LED is used to illuminate the contact angle.

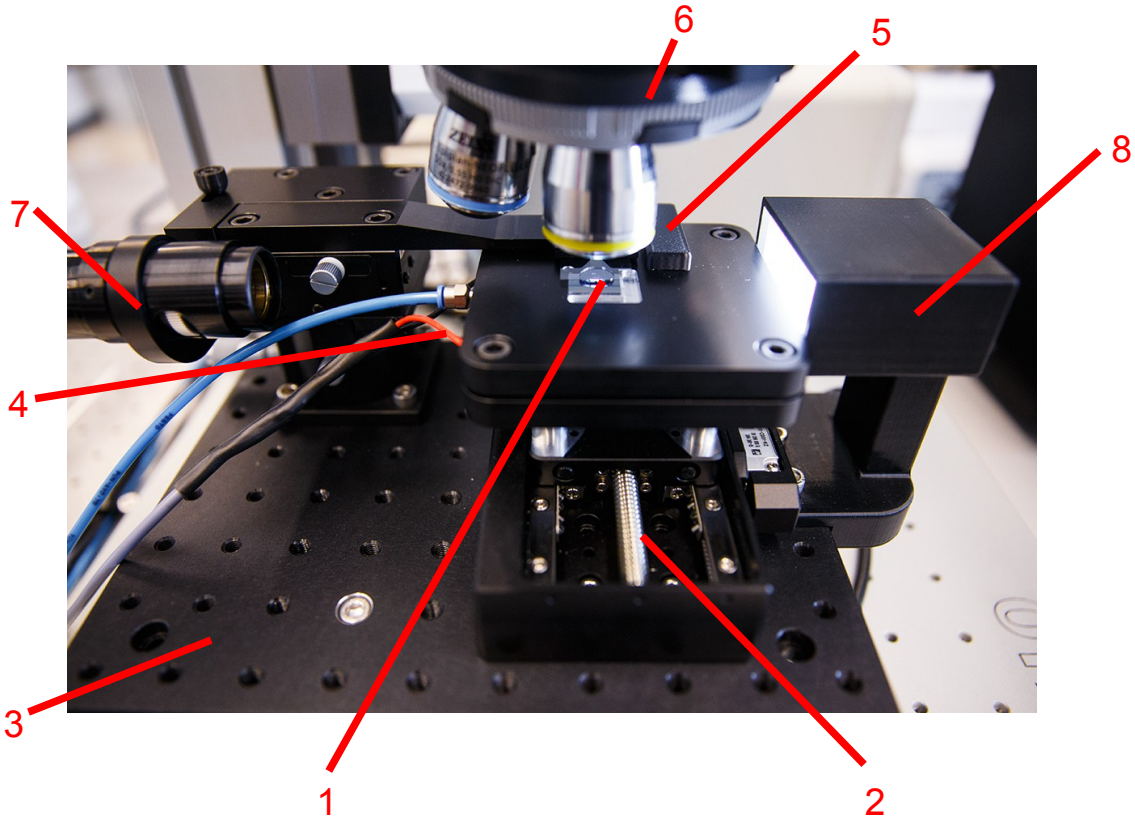

Figure 8 : Picture of the experimental setup.

4.1 Arduino shield

A previous Arduino shield (Figure 9 a)) has been designed by D. Bonzon (LMIS4) to drive the Peltier and the LED. However, the power supply doesn't deliver sufficient current for the Peltier (12 V DC, 5 A max.) and it wasn't possible to invert the polarity of the Peltier without doing it manually. Hence, a design is proposed with an additional H-bridge from Infineon and the connector for a power supply that can deliver an higher current (12 V DC, 10 A max.).
A first prototype has been done (Figure 9 b)) and, by connecting a resistance of 5 Ω to the H-bridge, a voltage drop of 11.8 V across the resistance was measured. Moreover, the polarity was successfully changed from the computer. However, when a Peltier element is connected, the voltage drop is lower than 2 V and the current going through the Peltier is below 2 A. The reason of this behavior may come from the H-bridge. A load short-circuit protection that can limit the current, is implemented with the H-bridge and the 1 Ω resistance of the Peltier can be seen as a short-circuit.

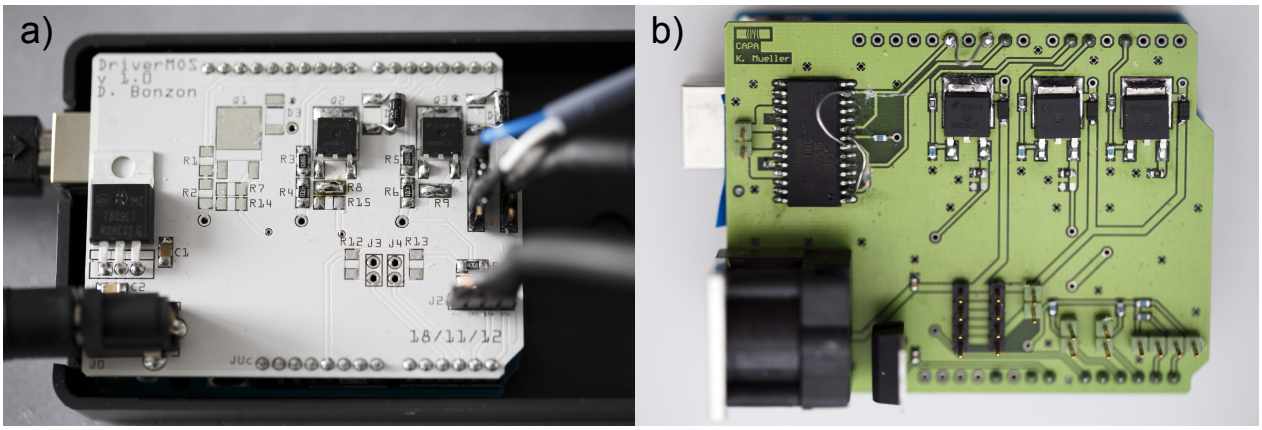

Figure 9 : a) Arduino shield designed by D. Bonzon b) Prototype of the new Arduino shield. The H-bridge is the integrated circuit at the top left corner of the board.

4.2 Labview program

To control most devices of the setup and to monitor the parameters with a single interface, a Labview program has been implemented. This program allows to control the 3 motors by using the interface or the keyboard, to turn off or on the LED and to control the Peltier. Moreover, the program monitors the temperature and humidity of the room and the temperature of the chip. All the data collected by the program can be saved in a text file that can be used to plot the data (Figure 10). A log has been implemented to write comments during the process and the comments are saved in the text file.

In the annexe, a complete description of the user interface and some useful information such as the text file format, Labview functions used in the program and the needed information to ensure the communication with external devices, is presented.

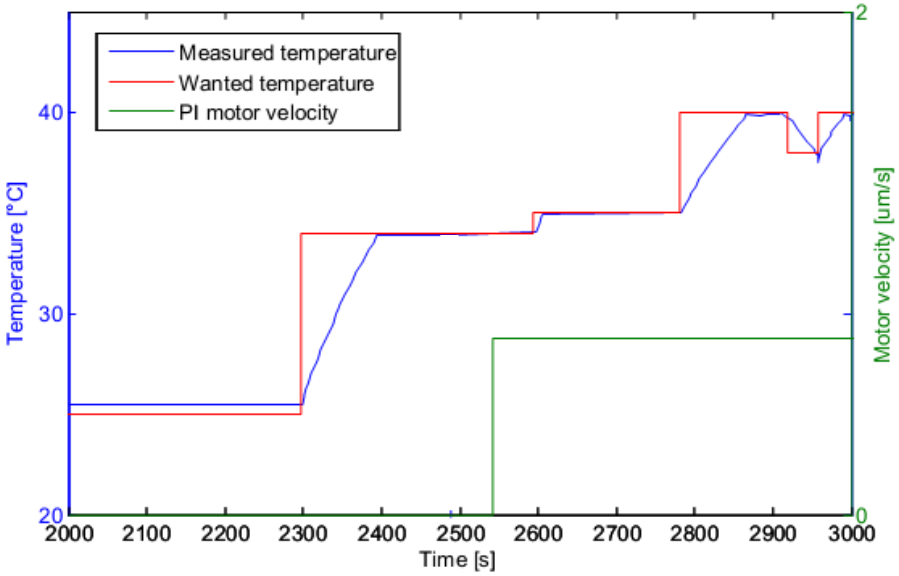

Figure 10 : Plot of the measured temperature, the wanted temperature and the PI motor velocity over time.

4.3 Product used in the CAPA

The nanospheres were purchased from Cytodiagnostics (item reference : CGA3K-50-50). The nanospheres have a diameter of 50 nm, is functionalized with amine group and the concentration of nanospheres is $1.76 \cdot 10^{12}$ particles / ml. The surfactant used to decrease the contact angle is Sodium dodecylbenzenesulfonate (SDBS) with a molarity of 7.17 mM.

5. Process flow

Templates for the CAPA process are molded using Ormocer as a transparent UV-curable polymer and a silicon master chip as the template. To fabricate the nanostructured silicon chip, a silicon wafer is dryed using a hotplate at 200°C for 5 min., hydrogen silsesquioxane (HSQ, a negative resist) with a concentration of 2% or 4% is spun such that the thickness of the film is between 50 nm and 100 nm. Then, the wafer is exposed by e-beam lithography (Vistec EBPG5000) with a dose between 2500 and 3000 $\mu C/cm^2$. After the exposure, the contrast is enhanced by a post-exposure bake (200° C, 2 min.), the wafer is developed using tetramethylammonium hydroxide 25%(TMAH) during 2 min, is rinsed with DI water and the HSQ film is exposed to 1000W plasma for 5 min. to increase the density of the film. Then, the wafer is dry etched (STS Multiplex ICP) using chlorine gas with a etch rate 0.35 μm/min for a etch depth between 50 nm and 100 nm. The dry etching is for a longer mold reusability. Usually, a height of 70 nm gives a good assembly yield during the CAPA process. The fabrication of the silicon wafer is done by Valentin Flauraud.

To dice the glass wafer and the silicon wafer, the surface is activated by plasma and a protection film is spun. The plasma ensures a good adhesion of the protection layer. Then, the wafer is diced into 17 x 17 mm^2 chip (Disco DAD321) and the protective layer is removed by wet etching using Remover 1165 from Shipley.

To reduce the adhesion of Ormocer on silicon, the silicon chip is activated by using a 1000W oxygen plasma for 2 minutes (Tepla 300) and the chip is placed in a desiccator with a droplet of Trichloro(1H, 1H, 2H, 2H-perfluoro-octyl)silane .The glass chip is well cleaned using oxygen plasma (Tepla 300) to improve the adhesion of Ormocer on the chip. For the molding, a droplet of Ormocer is placed on the silicon chip followed by the glass chip. Then, pressure is applied on the glass chip to spread the Ormocer over the silicon chip, the pressure is released and the Ormocer between the silicon chip and the glass chip rests for 5 min. before exposing the Ormocer to UV light. To cross-link the Ormocer, the exposure time is 15 min and the demolding process is done by using two tweezers. After molding, a 50nm-thick metal layer (aluminum or chromium) is deposited on the backside by sputtering (Alliance-concept DP 650). This layer allows to find easily the position of the structures with a microscope under dark-field illumination. Then, the glass chip is hard baked at 150° for, at least, 4 hours in order to stabilize and further cross-link the Ormocer. Finally, the surface of the Ormocer is activated by a 29W oxygen plasma for 20 seconds at a pressure of 200 mbar (plasm Harrick) and silanized (Trichloro(1H, 1H, 2H, 2H-perfluoro-octyl)silane, at least 3 hour in a dessicator). After the CAPA, the metal film on the backside of the ship is removed using a ion beam etcher (Veeco Nexus IBE350).

6. Design consideration & results

6.1 CAPA in practice

As CAPA is a non steady-state process for, mainly, two reasons. The surfactant concentration changes over time because of the evaporation of water and, if the humidity and temperature isn't well controlled, the dew point isn't same between two different CAPA leading to a different evaporation rate even if the temperature of the liquid is the same. To compensate the effect of the variation of the surfactant concentration leading to smaller contact angle, the temperature of the chip has to decrease because a lower evaporation rate increases the contact angle by decreasing the accumulation region. This control can be done because the contact angle and the accumulation region is monitored. However, the temperature can't be lower than the temperature of the room due to setup limitations so the initial concentration of surfactant has to be chosen such that the CAPA is still good at the end of the assembly. A general rule is to lower slightly the surfactant concentration when the dew point is lower in order to increase the contact angle.

When the drop of the colloid is placed between the chip and the slide, the drop should not touch the edge of the chip to avoid that the colloid unpins from the edge of the moving slide instead of the edges of the chip.

6.2 First design

The objective of this design is to perform fluorescence enhancement experiments with controlled gap size. Hence, for the mask design, 2 squares of 70 x 70 nm^2 representing the holes where the gold nanospheres will be trapped, is linked by a bridge with a width of 40 nm (Figure 11). The varying parameters are the length of the bridge and the orientation of the structures. The purpose of the bridge is to allow fluorescent dye to reach the hot spot of the plasmonic structure. Additional squares of different size has been done for characterization purpose.

Figure 11 : The different patterns used in the first design.

At the end of the process, the shape is well conserved (Figure 12) but the size of the structures is around 40 nm larger than the structure on the silicon chip, leading to multiple nanospheres for one hole (Figure 13). The effect of plasma on the dilatation has been investigated by comparing the pattern on the Ormocer before and after the plasma (Figure 14). It seems that the size difference is around 10 nm but, due to charging effects, this difference is too small to conclude that the plasma widens the hole in a significant way. For the CAPA, 60 µl of DI water and 20 µl of SDBS (dilution 1:20) are added to 30 µl of gold colloid. The speed is set to 0.7 µm/s and the temperature of the chip during the process is shown in the Figure 15. The temperature of the chip must decrease during the CAPA to prevent the deposition of particles outside the patterns. The temperature and the humidity of the room were 23.9°C and 29.8 % relative humidity. Hence, the

dew point was 5.19 °C.

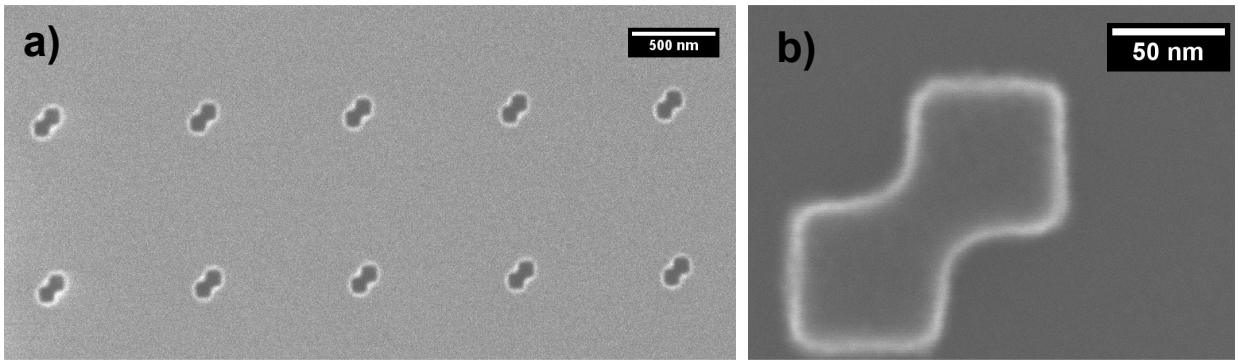

Figure 12 : a) SEM image from the secondary electron detector of a molded pattern on Ormocer.
b) SEM image from the InLens detector of the structure on the silicon chip.

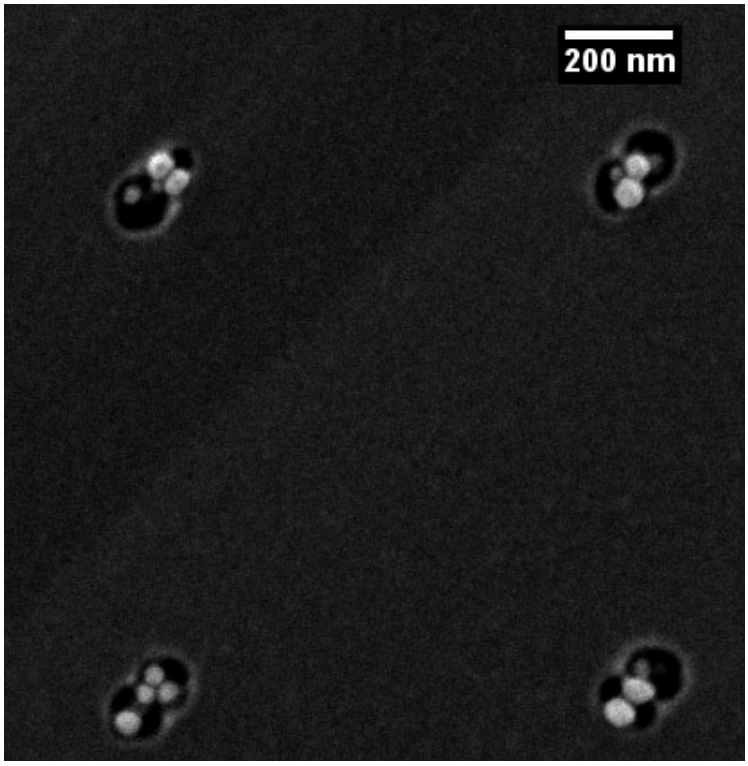

Figure 13 : SEM image from the secondary electron detector of a molded pattern on Ormocer filled with gold nanospheres.

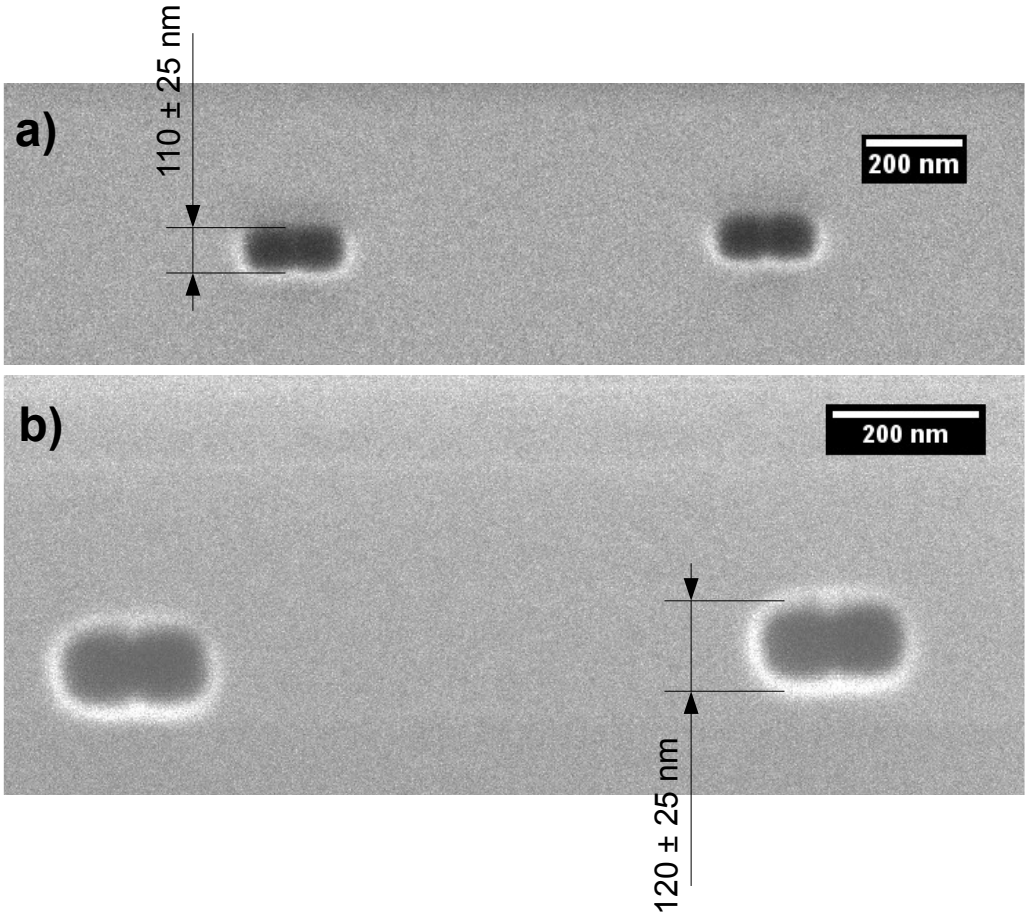

Figure 14 : SEM images from the secondary electron detector of the structures on Ormocer. a) Structure size before the plasma. b) Structure size after the plasma.

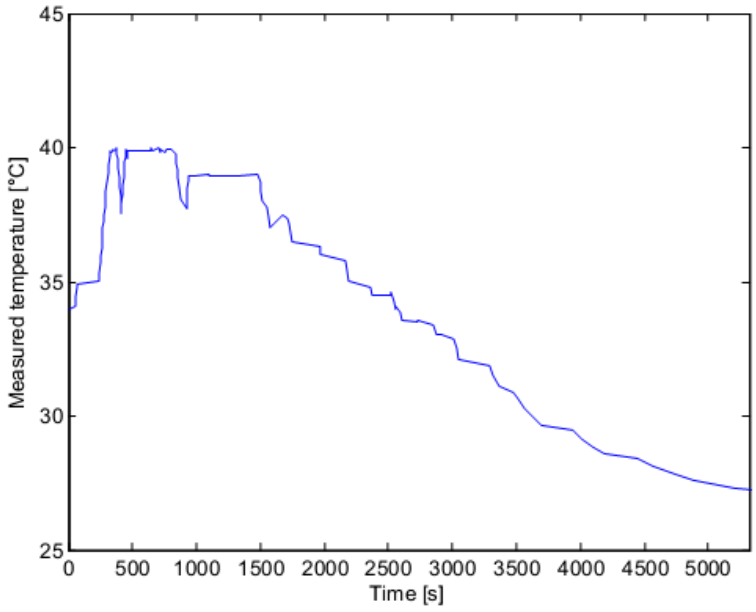

Figure 15 : Temperature of the chip along the experiment.

6.3 Second design

The objective of this design is to observe the plasmonic effect of a line of 2 to 10 particles and to assess confinement on a more simple structure. Therefore, the mask pattern consists of rectangles with a width of 70 nm and different length. As the first design, the structures at the end of the process are too wide, but the particles are still well aligned (Figure 16). For the CAPA, 20 µl of SDBS (dilution 1:20) is added to 50 µl of gold colloid. The temperature and the humidity of the room were 25.3°C and 21.2 % relative humidity. Hence, the dew point was 1.55 °C.

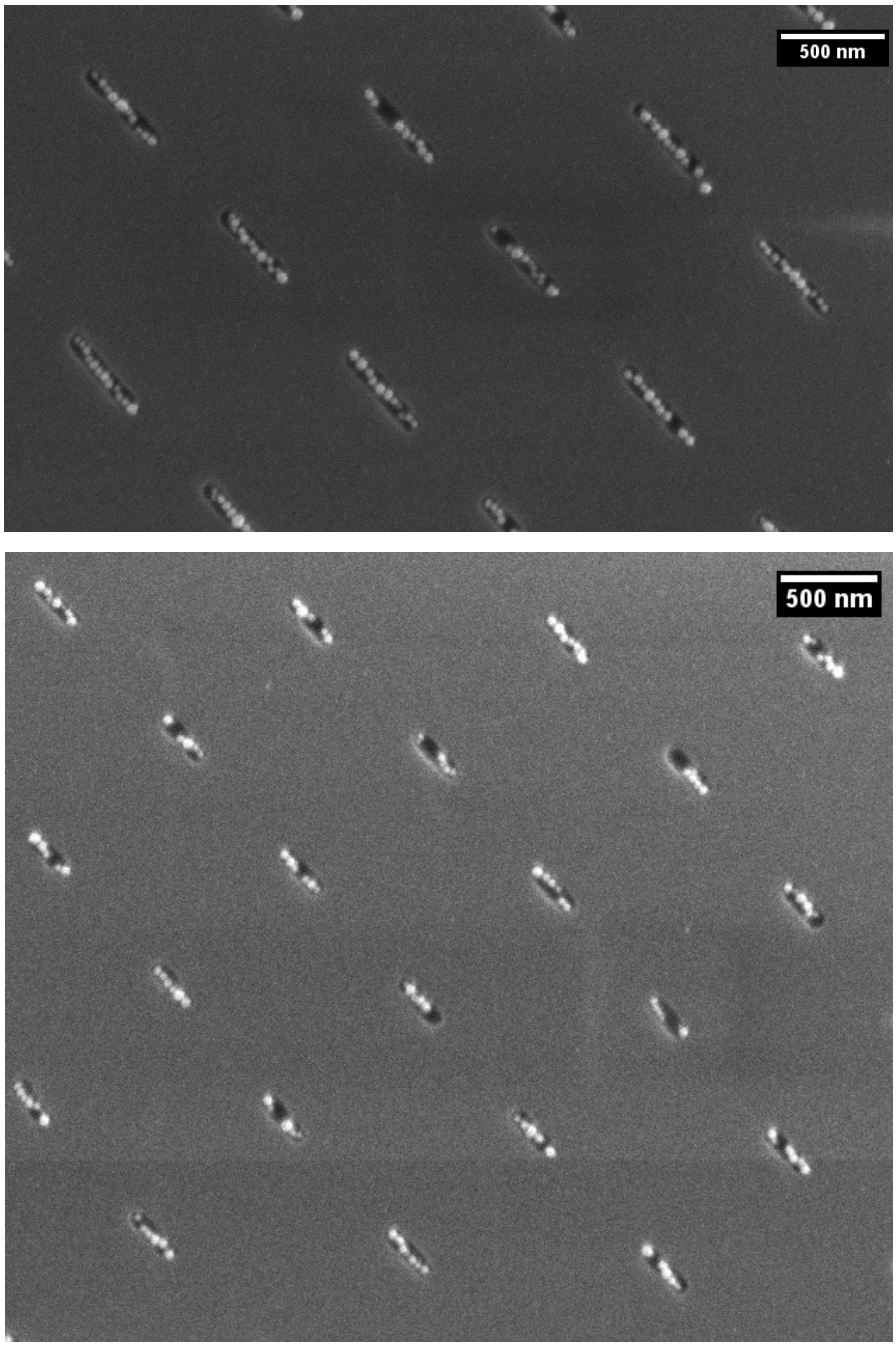

Figure 16 : SEM image from the secondary electron detector of a molded pattern on Ormocer filled with gold nanospheres.

6.4 Ormocer and Ormostamp

An advantage of using an hydrophobic Ormostamp instead of Ormocer is that the plasma following by the silanization step may not be needed. However, the CAPA with the use of colloid without surfactant fails because the receding contact angle was too low and the gold nanospheres were deposited everywhere on the chip. Hence, the use of Ormostamp wasn't investigated in this work.

6.5 Structure damage during molding

The molding was done using glass chips with a thickness of 0.55 mm or glass slide with a thickness of 1 mm. When the glass slide was used, the structure in the Ormocer was damaged (Figure 18). Two reasons can lead to this difference :

- The glass slide bends less than the glass chip during the demolding process resulting to a higher force at the edge of the structure when the glass slide is used.
- The technique used to demold is different (Figure 17) and the forces in presence during the demolding porcess may be higher when the glass slide is used.

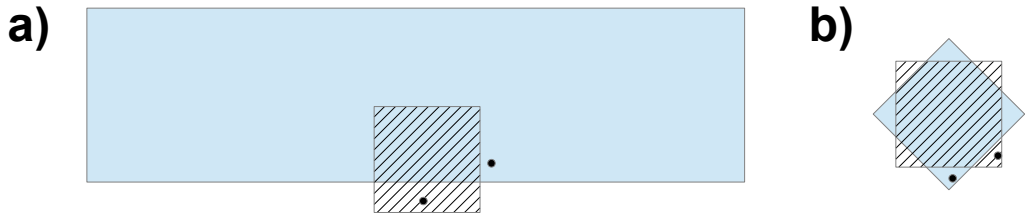

Figure 17 : Position of the silicon chip (hatched area) and the glass slide (a) or the glass chip (b) (light blue area) before demolding. During the demolding process, the forces is applied close to the black points.

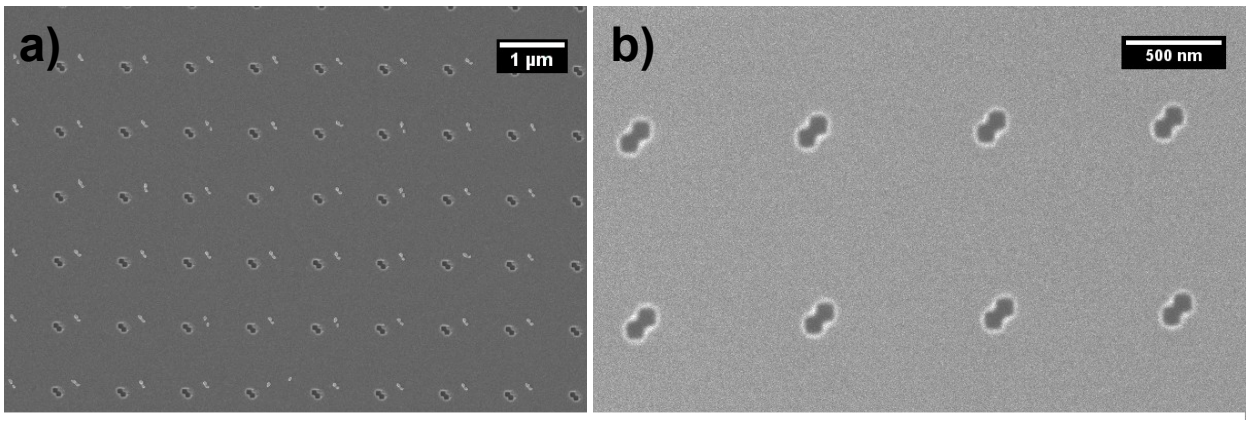

Figure 18 : a) SEM image from the InLens detector of structures on Ormocer. The Ormocer layer is on a glass slide. For imaging purpose, a 21 nm-thick layer of gold was sputtered. b) SEM image from the secondary electron detector of structures on Ormocer. The Ormocer layer is on a glass chip.

6.6 Repetitive molding with the same master chip

Multiple molding have been done on the same chip to test the re-useability of silicon chips. The SEM image has been done on the chip after the 1st molding and the 6th molding (Figure 19). After the 6th molding, no damage has be done on the silicon chip. However, Ormocer can lay on the silicon chip at the border of the molded area or because of bubble during the molding process. This Ormocer residue can lead to difficulties for the following molding process because the Ormocer tends to stick on the previously deposited Ormocer residue.

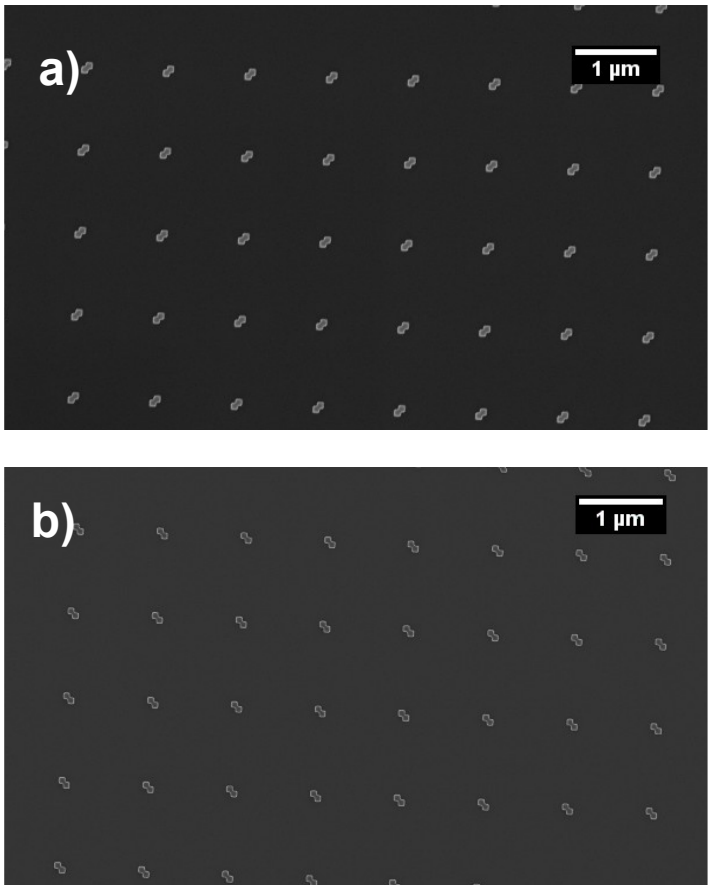

Figure 19 : SEM image from the InLens detector of a silicon chip. a) After the 1st molding process. b) After the 6th molding process.

7. Conclusion

In this work, a process for the fabrication of structures on Ormocer has been done, which, compared to top-down process using e-beam lithography or focused ion beam milling, is cost efficient and has a high throughput. Moreover, the patterned surface is transparent enabling plamonic experiments in transmission. The shape of the structures are close to the desired shape but the size of the structure are slightly larger leading to several nanospheres in one hole after the CAPA. Hence, the process gives good result but it needs to be repeated with molds of smaller dimensions.

In parallel, the experimental setup for the CAPA has been improved with a Labview program that

allows to control in a convenient way the different motors and monitor some important parameters. Moreover, a new Arduino shield has been designed but it seems that the H-Bridge limits the current that goes through the Peltier.

8. Outlook

To find the origin of the structure widening, a better characterization has to be found. One of them is to do a cross-sectional image in order to find how the process shapes the structure. The cross-section of a metal field Ormocer would enable to overcome the charging effect allowing the feature size measurement with a improved accuracy. Moreover, different polymer such as Omrocomp or Omrostamp can be tested in order to find a better polymer for the process. Once the structure can trap the desired number of particles, more complex shape or arrangement can be done such as asymetric structure or 2D-plasmonic crystal.

9. References

[1]Kraus, T., Malaquin, L., Schmid, H., Riess, W., Spencer, N. D., & Wolf, H. (2007). Nanoparticle printing with single-particle resolution. *Nature nanotechnology*, *2*(9), 570-576.

[2]De Gennes, P. G. (1985). Wetting: statics and dynamics. *Reviews of modern physics*, *57*(3), 827.

[3]Buck, A. L. (1981). New equations for computing vapor pressure and enhancement factor. *Journal of Applied Meteorology*, *20*(12), 1527-1532.

[4]Malaquin, L., Kraus, T., Schmid, H., Delamarche, E., & Wolf, H. (2007). Controlled particle placement through convective and capillary assembly. *Langmuir*, *23*(23), 11513-11521.

[5]Kuemin, C., Stutz, R., Spencer, N. D., & Wolf, H. (2011). Precise placement of gold nanorods by capillary assembly. *Langmuir*, *27*(10), 6305-6310.

[6]Cui, Y., Björk, M. T., Liddle, J. A., Sönnichsen, C., Boussert, B., & Alivisatos, A. P. (2004). Integration of colloidal nanocrystals into lithographically patterned devices. *Nano Letters*, *4*(6), 1093-1098.

[7]Xia, Y., Yin, Y., Lu, Y., & McLellan, J. (2003). Template-assisted self-assembly of spherical colloids into complex and controllable structures. *Advanced Functional Materials*, *13*(12), 907-918.

[8]Rivera, T. P., Lecarme, O., Hartmann, J., Rossitto, E., Berton, K., & Peyrade, D. (2008). Assisted convective-capillary force assembly of gold colloids in a microfluidic cell: Plasmonic properties of deterministic nanostructures. *Journal of Vacuum Science & Technology B*, *26*(6), 2513-2519.

[9] S. Maier, “Plasmonics: Fundamentals and Applications”, Springer (2007)

[10]Prodan, E., & Nordlander, P. J. C. P. (2004). Plasmon hybridization in spherical nanoparticles. *The Journal of chemical physics*, *120*(11), 5444-5454.

[11]Thyagarajan, K., Rivier, S., Lovera, A., & Martin, O. J. (2012). Enhanced second-harmonic generation from double resonant plasmonic antennae. *Optics express*, *20*(12), 12860-12865.

[12]Zhang, W., & Martin, O. J. (2010, August). Optical trapping and sensing with plasmonic dipole antennas. In *SPIE NanoScience+ Engineering* (pp. 775712-775712). International Society for Optics and Photonics.

[13]Kinkhabwala, A., Yu, Z., Fan, S., Avlasevich, Y., Müllen, K., & Moerner, W. E. (2009). Large single-molecule fluorescence enhancements produced by a bowtie nanoantenna. *Nature Photonics*, *3*(11), 654-657.

[14]Punj, D., Mivelle, M., Moparthi, S. B., van Zanten, T. S., Rigneault, H., van Hulst, N. F., ... & Wenger, J. (2013). A plasmonic/antenna-in-box/'platform for enhanced single-molecule analysis at micromolar concentrations. *Nature nanotechnology*, *8*(7), 512-516.

[15]Sivis, M., Duwe, M., Abel, B., & Ropers, C. (2013). Extreme-ultraviolet light generation in plasmonic nanostructures. *Nature Physics*, *9*(5), 304-309.

[16]Nakayama, K., Tanabe, K., & Atwater, H. A. (2008). Plasmonic nanoparticle enhanced light absorption in GaAs solar cells. *Applied Physics Letters*, *93*(12), 121904.

[17]Acuna, G. P., Möller, F. M., Holzmeister, P., Beater, S., Lalkens, B., & Tinnefeld, P. (2012). Fluorescence enhancement at docking sites of DNA-directed self-assembled nanoantennas. *Science*, *338*(6106), 506-510.

[18]Kern, A. M., Meixner, A. J., & Martin, O. J. (2012). Molecule-dependent plasmonic enhancement of fluorescence and Raman scattering near realistic nanostructures. *Acs Nano*, *6*(11), 9828-9836.

[19]Kinkhabwala, A., Yu, Z., Fan, S., Avlasevich, Y., Müllen, K., & Moerner, W. E. (2009). Large single-molecule fluorescence enhancements produced by a bowtie nanoantenna. *Nature Photonics*, *3*(11), 654-657.

[20]Hohenester, U., & Trügler, A. (2012). MNPBEM–A Matlab toolbox for the simulation of plasmonic nanoparticles. *Computer Physics Communications*, *183*(2), 370-381.

[21]De Abajo, F. G., & Howie, A. (2002). Retarded field calculation of electron energy loss in inhomogeneous dielectrics. *Physical Review B*, *65*(11), 115418.

[22]De Abajo, F. G. (2010). Optical excitations in electron microscopy. *Reviews of modern physics*, *82*(1), 209.

[23]Johnson, P. B., & Christy, R. W. (1972). Optical constants of the noble metals. *Physical Review B*, *6*(12), 4370.

[24]Chang, C. C., Yang, Y. T., Yang, J. C., Wu, H. D., & Tsai, T. (2008). Absorption and emission spectral shifts of rose bengal associated with DMPC liposomes. *Dyes and Pigments*, *79*(2), 170-175.

10. Annexe

10.1. Labview program

10.1.1 External devices

The program communicates with the following external devices :

- PI motor : It is connected to the port COM3.
- Standa x-y motors : If more than two Standa motors are connected to the computer, the program will communicate with only two of them. The others are ignored.
- Arduino Uno : It is connected to the port COM7. If the Arduino doesn't respond, the Arduino may be not configured properly. To do that, open Labview, go to "Tools→LabVIEW Hacker→LINX→LINX Firmware wizard" then select "Arduino" for the device family, "Uno" for the device type and "Serial/USB" for the firmware program interface. Click "Next" and select "COM7". Then, click "Next" two times and the Arduino will be configured.
  - Peltier : It is connected to the digital pin 3 of the Arduino.
  - LED : It is connected to the digital pin 5 of the Arduino.
  - Stage temperature sensor : It is connected to the analog input pin A4 and A5 of the Arduino.
- Room temperature and humidity sensor (Thorlabs USB key) : If more than one Thorlabs USB keys are connected to the computer, only one of them is read by the program. The others are ignored.

If one of them is connected to an other port of the computer or an other pin of the Arduino, it is possible that the program code has to be changed in order to work properly.

10.1.2 Data file

The program collect the following data :

- The temperature of the stage
- The wanted temperature
- The travel speed of the PI motor during the process. The travel speed is considered as 0 if the process isn't running.
- The room temperature.
- The room humidity
- The log

For each data, an integer indicates the number of data points followed by the data or the comments. Each data point is represented by the time from the beginning of the program in seconds and the data in degrees for the temperatures, in percent for the humidity and in micrometer per second for the travel speed. Each comment is preceded by the time from the beginning of the program in seconds and by the number of characters in the comment. Each values are separated by a space and each data point is separated by a new line.

10.1.3. Interface description

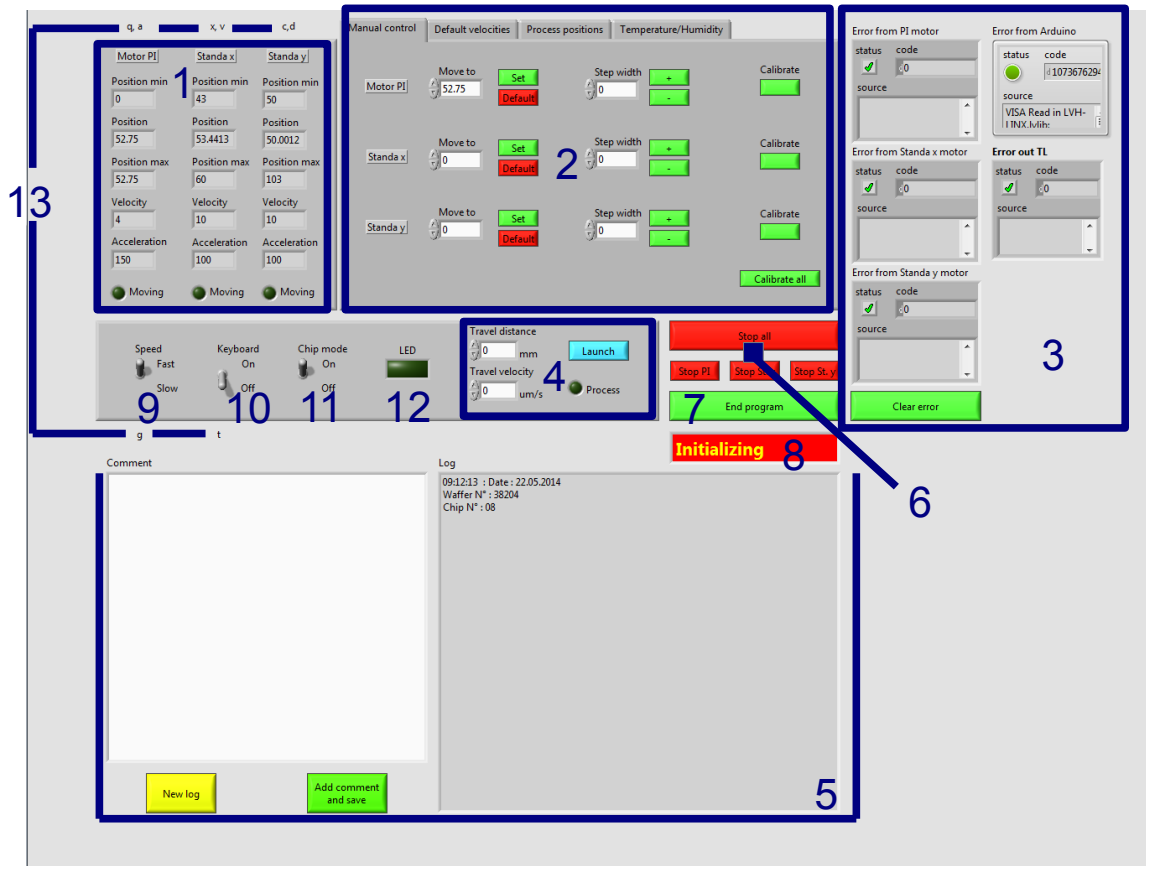

Figure 20 : User interface of the program.

Description of the user interface (Figure 20) :

1 : The actual state of each motor is shown in this panel. It includes the current position, velocity and acceleration of the motors, if the motor is moving and the limit positions of the motors. Those values are updated each 500 ms. The units are millimeter and second.

2 : It contains 4 panels : “Manual control”, “Default velocities”, “Process positions” and “Temperature/Humidity”. Each of them is described separately below.

3 : If the program runs normally, those elements are invisible. If there is an error in the program due to an external device, the corresponding error panel will show up along with the “Clear error” button. Clicking on the “Clear error” button will turn the button invisible along with the error panels. If the process is running, the “Clear error” button is deactivated. “Error TL” corresponds to the Thorlabs USB key that reads the temperature and the humidity of the room. “Error from Arduino” corresponds to the Peltier and the sensor that measures the temperature of the stage.

4 : In “Travel velocity” and “Travel distance”, the velocity of the PI motor and the distance travelled during the process can be set. It is advised to set a travel distance larger than needed. Clicking on the “Launch” will start the process and most of the buttons will be deactivated. The exception are the “Stop” buttons, the “End program” button and the “Add comment and save” button. When the process is ongoing, the “Process” indicator is on.

5 : By clicking the “Add comment and save” button, the actual time and the text in the “Comment” text-box are added to the log and the data in memory are saved. The keyboard is deactivated when the “comment” text-box is selected. By clicking the “New log” button, all the data in memory and the log are cleared. For both button, if the path to the data file isn't set, a window asks the user to select the location and the name of the data file. It is advised to save the data regularly to decrease the inconvenience due to a crash of the program.

6 : With those buttons, a single motor or every motor can be stopped. The reaction time is 50 ms maximum.

7 : By clicking on the “End program” button, all the motors are stopped, the LED and the Peltier are turned off, all communications are closed and the program ends. If the path to a data file isn't set, a window asks the user to select the emplacement and the name of the data file.

8 : When the “Initializing” flag is visible, the user can't interact with the program.

9 : This interrupter allows to select the velocities of the motors (slow or fast). The values of those velocities are set in the “Default velocities” panel. At the beginning of the program, the velocities are set to fast.

10 : This interrupter allows to activate or deactivate the keyboard. At the beginning of the program, the keyboard is deactivated.

11 : This interrupter allows to change the Standa motor limit positions. The area is smaller when the chip mode is activated (Figure 21). At the beginning of the program, the chip mode is activated.

12 : The button controls the LED.

13 : Those letters indicate the key used in the program : “q”,”a” for the PI motor, “x”,”v” and “d”,”c” for the Standa motors, “g” to change the speed (slow or fast) and “t” to deactivate the keyboard. The keyboard can't be activated by using the keyboard.

10.1.3.1. “Manual control” panel

Description of the “Manual control” panel(Figure 22) :

1 : By clicking the “Set” button, the corresponding motor moves to the indicated position written in the text-box. The “Default” button replaces the value in the text-box by the current position of the motor.

2 : By clicking on the “+” or “-” button, the motor moves by a step indicated in the corresponding text-box. The Figure 21 indicates which is the positive and the negative direction.

3 : By clicking on the “Calibrate” button, the corresponding motor will move to the minimum position and set the position to 0. By clicking on the “Calibrate all” button, the PI motor is calibrated. At the same time, the Standa-y motor is calibrated followed by the Standa-x motor. If the motors don't move properly when the keyboard or the step move is used, it usually means that the motors need to be calibrated.

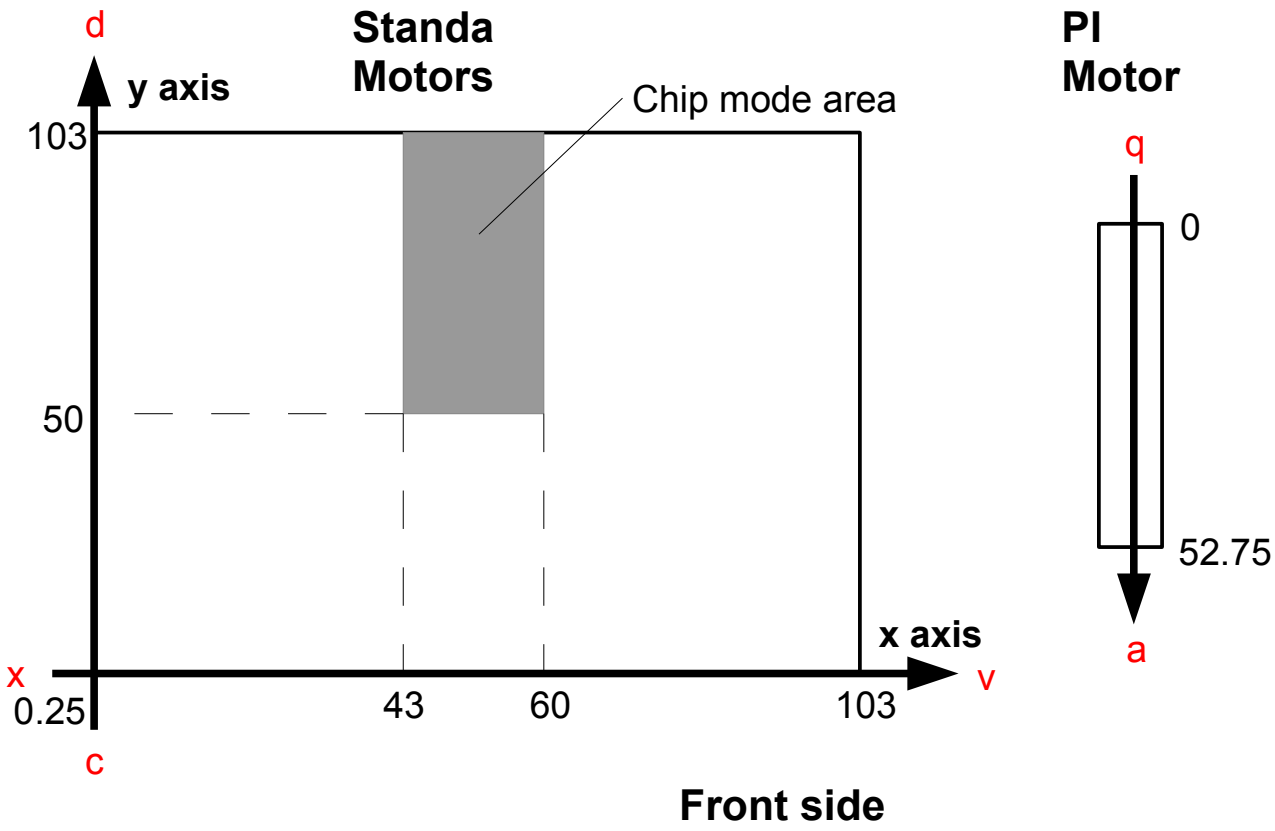

Figure 21 : Schematic of the degrees of freedom of the motors. The values written on the axis are in millimeter and corresponds to the limits of the motor for the chip mode area and the full range area. The letters in red correspond to the key used to move the different motors.

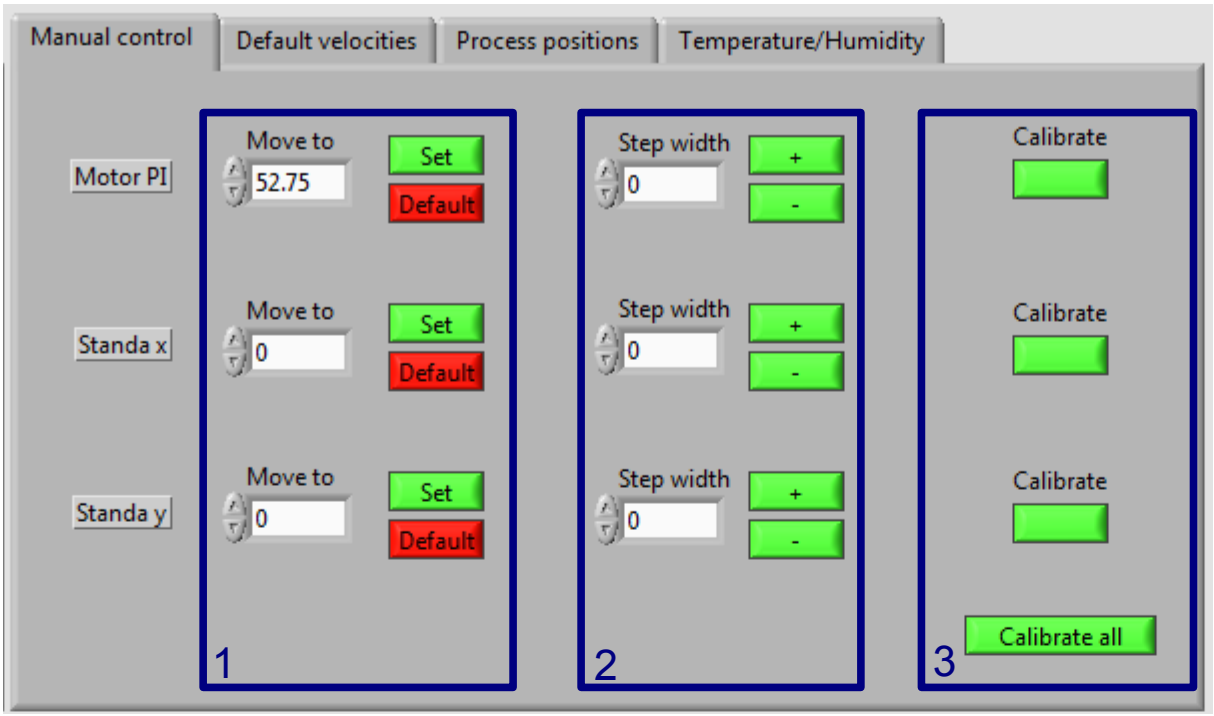

Figure 22 : “Manual control” panel.

10.1.3.2. “Default velocities” panel

Description of the “Default velocities” panel (Figure 23) :

1 : The text-boxes indicate the fast and slow velocities for each motor. When one of those values is changed, the velocity of the corresponding motor may change only if the motor is stopped. At the beginning of the program, the values of the velocities are as written in the figure 23.

2 : By clicking the “Set” button, the acceleration of the corresponding motor is set to the value indicated in the text-box The “Default” button replaces the values in the text-box by the current acceleration of the motor.

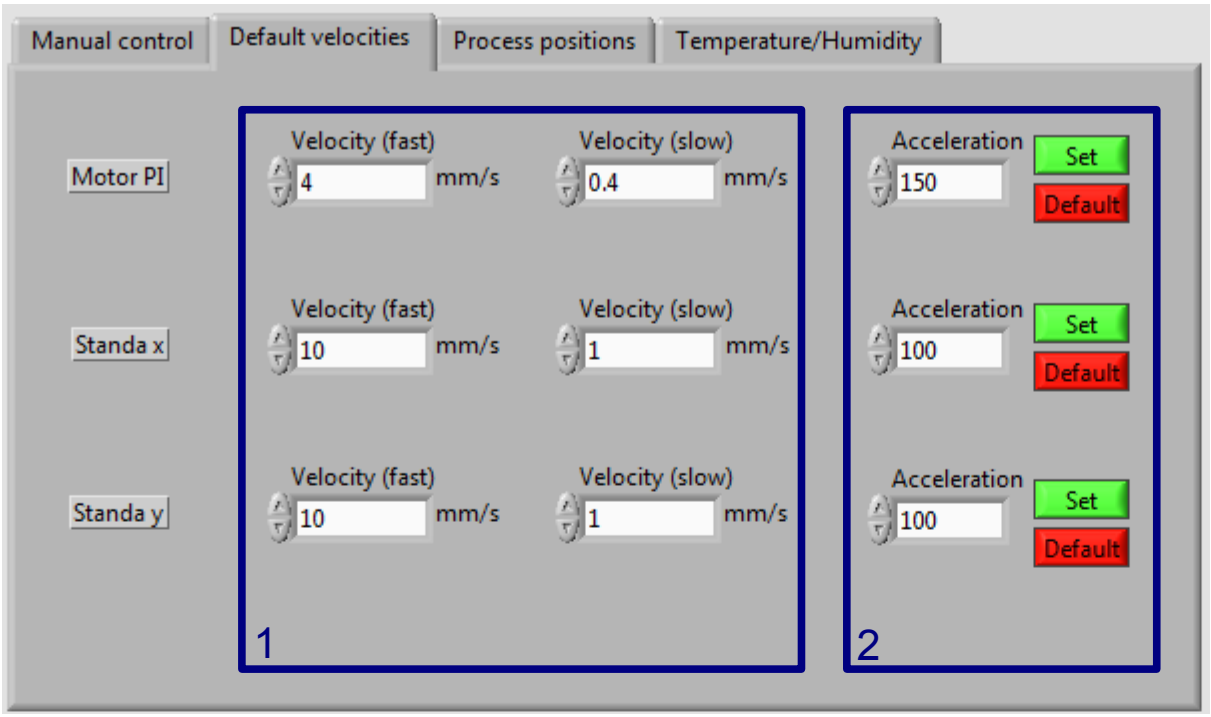

Figure 23 : “Default velocities” panel.

10.1.3.3 “Process positions” panel

Description of the “Process positions” panel (Figure 24) :

1 : By clicking on the “Set start” button, the current positions of the motors is set as the start position and are written in the “Position PI”, “Position St.x” and “Position St.y” text-boxes. By clicking the “To start position” button, the motors move to the start position. By clicking on the “Set end” button, the difference between the position written in the “Position PI” text-box and the current position of the PI motor is written in the “Travel distance” text-box (Figure 20).

2 : By clicking on the “Home” button, the PI and the Standa-y motors move to the nearest position from the front side (Figure 21).

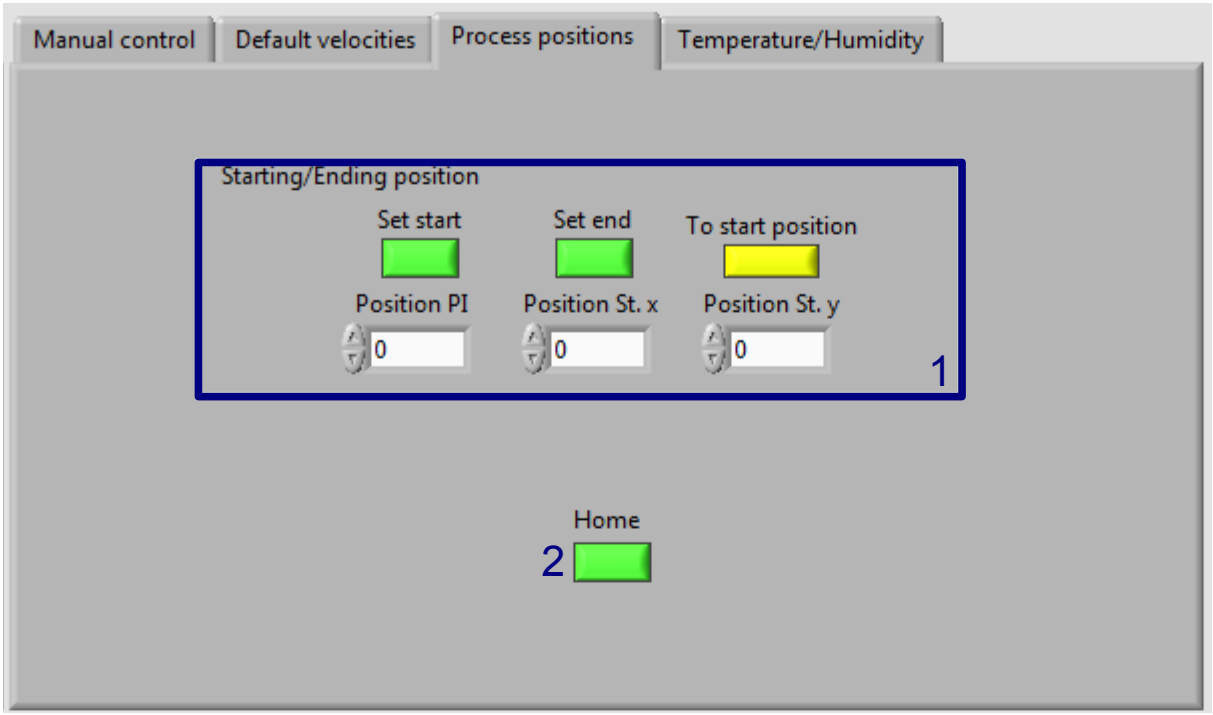

Figure 24 : “Process positions” panel.

10.1.3.4. “Temperature/Humidity” panel

Description of the “Temerature/Humidity” panel (Figure 25) :

1 : The room temperature and humidity measured by the Thorlabs USB key are shown in the “Room Temperature” and “Relative humidity (%)” text-boxes. From those values, the dew point is calculated using the following formula[3] :

$$\gamma(T, RH) = \ln\left(\frac{RH}{100}\right) + \frac{bT}{c+T}$$
$$T_{dp} = \frac{c\,\gamma(T, RH)}{b - \gamma(T, RH)} \qquad (7)$$
$$b = 17.368,\ c = 238.88\,^{\circ}C$$

Where T is the room temperature, RH is the relative humidity in percent and T_{dp} is the dew point.

2 : This text-box indicates the expected temperature of the chip. The temperature can be slightly different when a glass chip is used due to the low thermal conductivity of glass.

3 : Those text-boxes allow to set the desired temperature. By setting the “Reference” slide to “Absolute setpoint”, the “Delta to dew point” is updated every 500 ms and vice versa if the “Reference” slide is set to “Delta to dew point”. The relationship between “Dew point” (T_{dew}), “Absolute setpoint” (T_{abs}) and “Delta to dew point” ($T_{\Delta dew}$) is :

$$T_{abs} = T_{dew} + T_{\Delta dew} \qquad (8)$$

4 : The “Error” text-box indicates the difference between the “Absolute setpoint” and the “Chip temperature”.

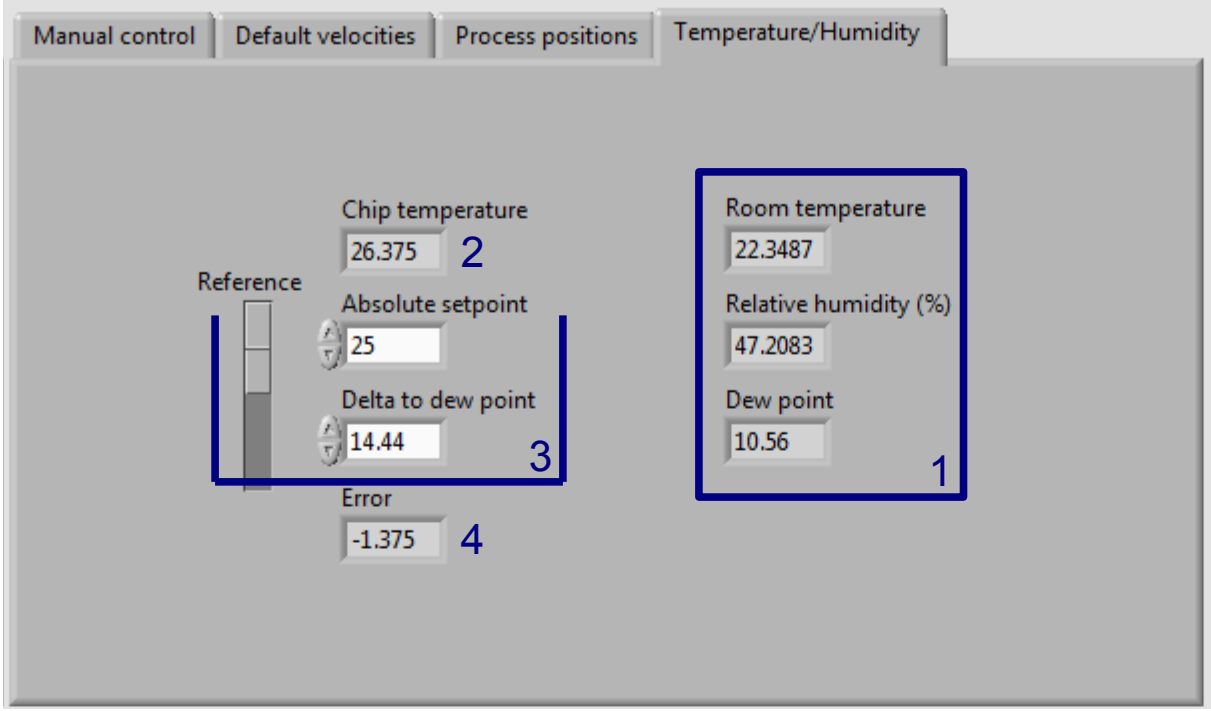

Figure 25 : “Temerature/Humidity” panel.

10.1.4 Program code

As mentioned before, it is possible that the program code needs a modification in order to work properly if an external device is connected to an other port of the computer or an other pin of the Arduino. The Figures 26 and 27 show where the ports of the computer or the pins of the Arduino are indicated.
Many functions have been implemented and they can be divided in 2 groups. The first group concerns the Standa motors and they control the movement, the velocity and the acceleration of the motor. The step of the Standa motors can be changed and it is important to reduce the step when the velocity is too slow. To do that, the function “Step control” sets the velocities where the step is changed.
The second group is for controlling the Peltier and saves the data (data to an array and array to a file). For the Peltier, the control loop is written in the “Control temperature” function. To save the data, there are 3 functions :

- “Save data step” : it saves the data in the array only if the input data changes. In this case, 2 data points are saved in the array : the previous and the current data. It isn't advised to use this function when the data change continuously.
- “Save data approx” : for each input data, this function finds the best lines to fit the data. The condition to start computing an other line is that the last data point is too far from the average of the data points used to compute the previous line.
- “Save data file” saves the arrays containing data and the log into a file.

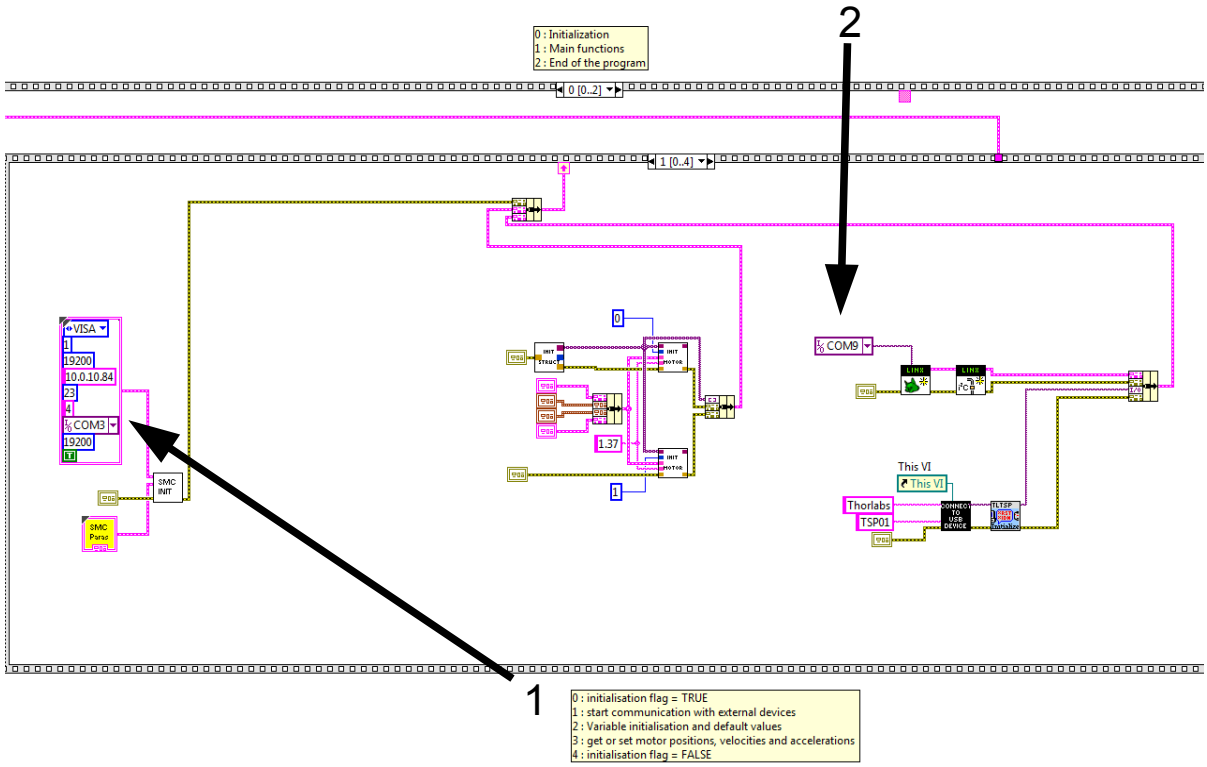

Figure 26 : Part of the code where the ports of the computer used for the PI motor (1) and the Arduino (2) are indicated. This part of the code is in the sequence 1 ("start communication with external devices) of the sequence 0 ("Initialisation").

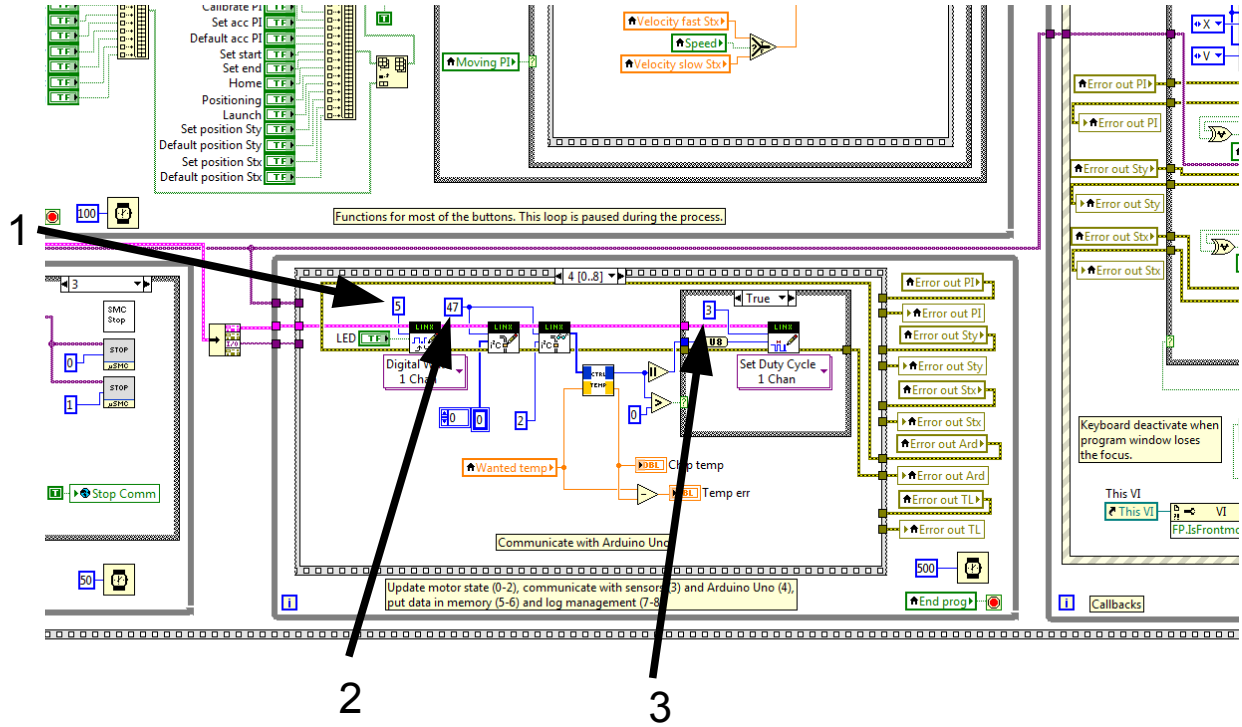

Figure 27 : Part of the code where the pins of the Arduino used for the LED (1), the temperature sensor (2) and the Peltier (3) are indicated. The pin of the Arduino for the temperature sensor is in hexadecimal. This part of the code can be found in the sequence 4 ("Arduino Uno") of the sequence 1 ("Main functions").